Progress In Electromagnetics Research C, Vol. 90, 29–39, 2019

A Novel Dual-Passband Net-Shaped FSS Structure Used for MIMO Antennas

Zhiwei Liu*, Shunli Jie, Haitao Ma, Xiaoyan Zhang, and Beibei Xing

Abstract—A dual-passband frequency selective surface (FSS) is designed in this paper. Two passbands are 2–3.4 GHz and 5.5–6.8 GHz, respectively. It is used as a spatial filter to improve the radiation and scattering performance of an antenna. The structure is combined with two layers. One is metal, and the other is intermediate medium. The requirements of wide-band, polarization-independent, wide incidence angle and miniaturized FSS with a thickness of only 0.0085λ are achieved by parameter optimization. When the FSS is used to the proposed microstrip antenna, the relative bandwidth is increased by 31.4% and 50%, and the peak gain is increased by 2.53 dB and 1.86 dB at 5.8 GHz and 6.4 GHz, respectively. Meanwhile, the maximum RCS reduction of the microstrip antenna is 16 dB. On the other hand, the FSS is able to be applied to a dipole antenna to improve the transmission coefficient and phase. Simulation and measurement results of the transmission coefficient and phase of the antenna are almost the same.

1. INTRODUCTION

Frequency selective surface (FSS) is a 2-D periodic array structure consisting of periodically arranged metal patch elements or periodically perforated metal screen elements [1–3]. It can be fabricated into frequency filters or polarization filters for radar stealth space filters or sub-reflector antennas. When the electromagnetic wave is incident on array periodic resonance unit, the induced current will be generated, and the scattered electromagnetic wave will be formed. If we analyze the circuit, according to the transmission line theory, the conductive patches and slots of the unit structure of the frequency selective surface can be equivalent to inductance and capacitance, respectively. It can be equivalent to an LC resonant circuit.

The main parameters that will determine the overall frequency response of an FSS include dielectric substrate properties, element shape geometry, inter-element spacing (cell-size or periodicity) and incidence angle of spatial waves on the surface [4–7]. Different FSS structures have been investigated by microwave engineers in the development of high performance spatial filters, such as reconfigurable frequency selective surfaces [11–14], multilayered selective filters [8], periodic arrays on anisotropic substrates [9, 10], and FSSs with geometric fractal elements [15–19].

When FSS is used to improve the performance of an antenna, it should cover the working frequency band of the antenna. Accordingly, some performance of the antenna can be enhanced significantly, such as relative bandwidth and peak gain. Although there is coupling action between the FSS and MIMO antenna, the effect can be reduced or reused to improve the performance by good optimization. This manuscript focuses on a double-layer net FSS structure with many characteristics including broadband, ultrathin, wide incidence angle, and stabilized polarization. When the proposed FSS is used to improve the performance of a microstrip antenna, the bandwidth and gain of the antenna are improved greatly. Besides, the radar cross section (RCS) of the antenna is obviously reduced in its working band. The characteristics of independent polarization, wide angle band and miniaturization can also be observed in our simulation and measurement results.

Received 15 October 2018, Accepted 14 December 2018, Scheduled 14 January 2019
* Corresponding author: Zhiwei Liu (zwliu1982@hotmail.com).
The authors are with the East China Jiaotong University, Nanchang 330013, China.

2. DESIGN AND ANALYSIS

2.1. High Performance FSS Design

First of all, the frequency of the designed FSS should be selected. As shown in Fig. 1, the Jerusalem cross is chosen as the basic unit structure here since the Jerusalem-type FSS unit has wide bandwidth and performs stably. A net-shaped FSS structure is obtained by optimizing and improving the Jerusalem cross. After that, the size of FSS unit is calculated according to the equivalent circuit and the formula of resonance frequency of FSS. Finally, the final structural parameters are obtained by modeling, simulation and optimization in the three-dimensional electromagnetic modeling software HFSS.

$$L = -\mu_0 \frac{p}{2\pi} \log\left(\sin\left(\frac{\pi\omega}{p}\right)\right) \tag{1}$$

$$C = -\varepsilon_0 \varepsilon_{eff} \frac{2p}{\pi} \log\left(\sin\left(\frac{\pi s}{2p}\right)\right) \tag{2}$$

$$f = \frac{1}{2\pi\sqrt{LC}} \tag{3}$$

where p, w and s represent the length, width and spacing of capacitance and inductance, respectively. ε_{eff} represents the effective dielectric constant of dielectric substrate. By combining Eqs. (1), (2), (3), the resonant frequency of the cross structure unit can be approximately calculated. In order to increase the bandwidth and decrease the size, a double-layer structure is adopted. The four branches on the back and front of the structure form a coupling capacitor, which reduces the resonance frequency and makes the design miniaturized. Finally, the final structural parameters are obtained by modeling, simulation and optimization in the three-dimensional electromagnetic modeling software HFSS.

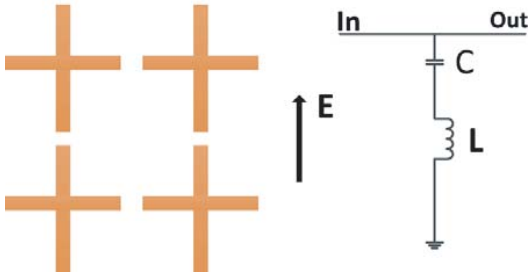

Figure 1. Cross structural units and its equivalent circuits.

Figures 2(a) and (b) show the top and back views of the FSS structure. Fig. 2(c) describes the array structure. The thickness can be seen in Fig. 2(d). Obviously, the structure is composed of two layers including metal and dielectric layers. FR-4 is used as the dielectric substrate with relative permittivity equal to 4.4 and loss tangent equal to 0.02. By analyzing the S parameters shown in Fig. 3, the working bandwidths of FSS are 2–3.4 GHz and 5.5–6.8 GHz, respectively.

In order to verify the high performance of the proposed FSS, the frequency response curves of TE and TM polarization waves at different incident angles are given in Fig. 4. It can be seen that the designed FSS resonates steadily around 2.5, 5.7 and 6.4 GHz with the increase of incident angle for both TE and TM polarizations. The bandwidth of FSS is 1.4 GHz, and the relative bandwidth is 51.8% when plane wave is incident vertically in low frequency. The results show that FSS has good stability for different polarizations and wide incidence angle in a wide frequency band.

According to the transmission line theory [14], the proposed FSS unit can be equivalent to the transmission line model shown in Fig. 5. Suppose that R_T is the characteristic impedance of the transmission line and that L and C are the equivalent inductance and capacitance of the proposed FSS.

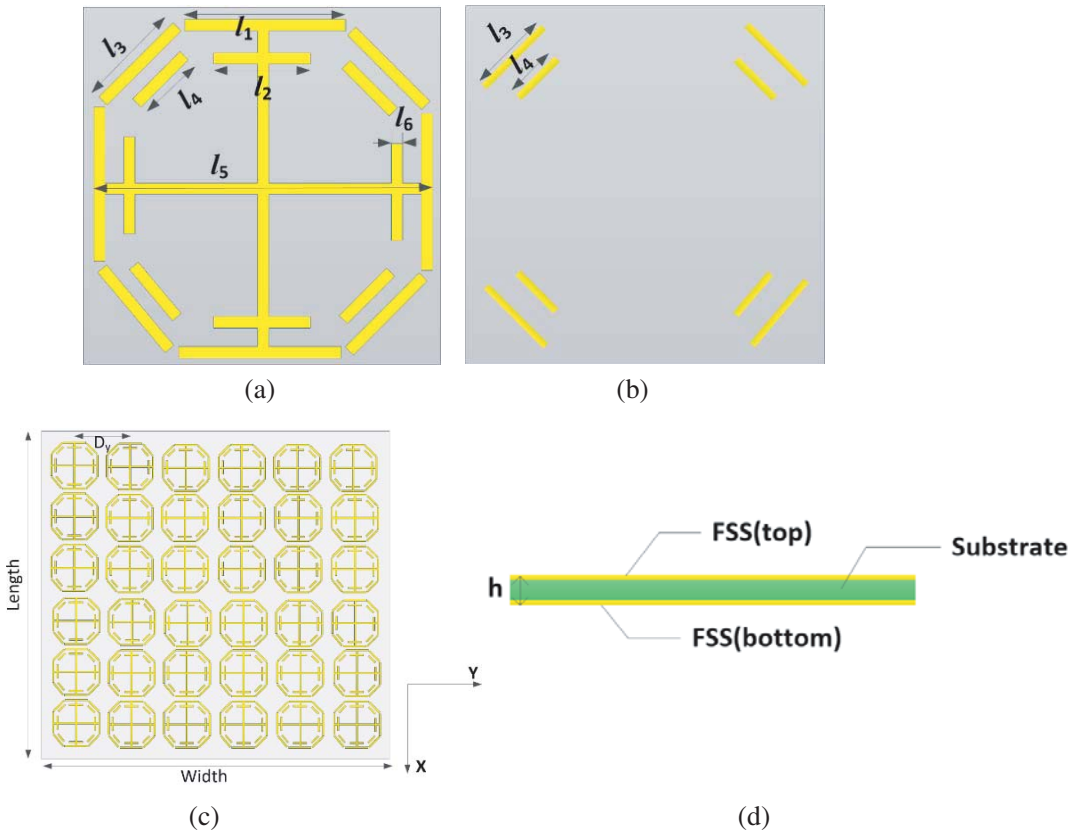

Figure 2. Configuration and parameters of the proposed FSS substrate: $l_1 = 20\,\text{mm}$, $l_2 = 10$ mm, $l_3 = 8\,\text{mm}$, $l_4 = 8\,\text{mm}$, $l_5 = 35\,\text{mm}$, $l_6 = 0.5\,\text{mm}$, $D_y = 37\,\text{mm}$, Length $= 230\,\text{mm}$, Width $= 230\,\text{mm}$. $h = 1.2\,\text{mm}$. (a) Top view. (b) Back view. (c) 6×6 FSS arrays. (d) Side view.

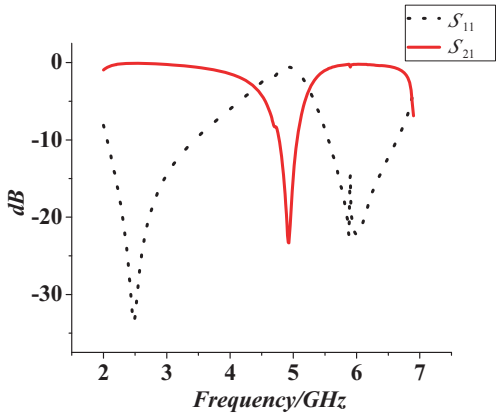

Figure 3. S_{11} and S_{21} curves of FSS.

The reflection coefficient can be shown in Eq. (4).

$$\Gamma = \frac{\dfrac{R_T\left(j\omega L + 1/j\omega C\right)}{R_T + j\omega L + 1/j\omega C} + R_T}{\dfrac{R_T\left(j\omega L + 1/j\omega C\right)}{R_T + j\omega L + 1/j\omega C} - R_T} = -\frac{R_T/2 + j\omega L + 1/j\omega C}{R_T/2} \tag{4}$$

where ω is the frequency of the incident electromagnetic wave. When the equivalent circuit works at

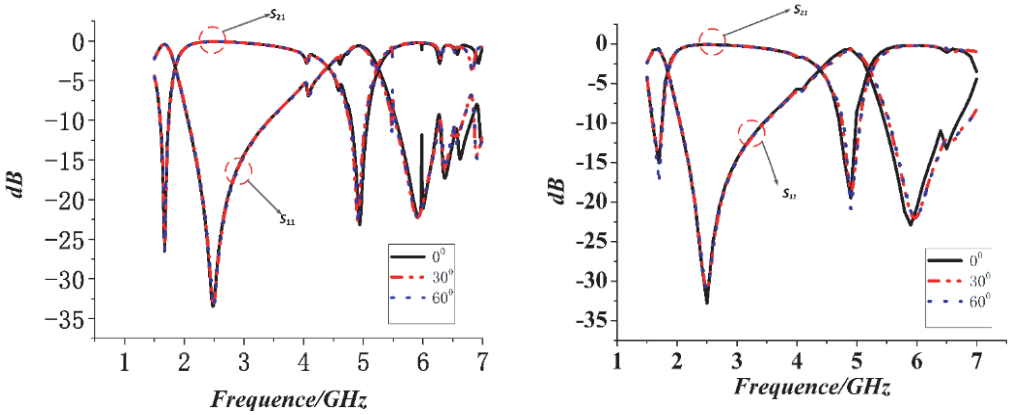

Figure 4. The curves of S_{11} under different polarization and incidence angles. (a) TE polarization. (b) TM polarization.

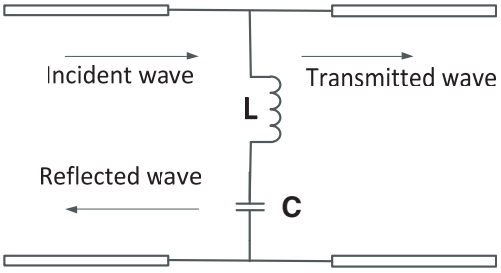

Figure 5. Equivalent model of FSS transmission line.

resonant frequency, the reflection coefficient will be zero according to Eq. (5).

$$j\omega L + 1/j\omega C = \frac{R_T}{2} \tag{5}$$

Thus, the frequency selective surface presents a band-pass characteristic.

2.2. Dual Band Microstrip Antenna With FSS

To investigate the performance of the FSS, a circular-shaped MIMO microstrip patch antenna is designed, as shown in Fig. 6. In this paper, circular patch antenna is selected and used due to its compact structure and wide bandwidth. According to the working frequency of the antenna, the size of the antenna is determined. The main purpose of slotting on the circular patch is to enlarge the length of the current path and reduce the size of the antenna. Finally, the structure parameters of the circular patch antenna are optimized by modeling and simulation in the electromagnetic software HFSS 15.

This antenna is excited by a coaxial cable with a 50 Ω SMA connector. The material of dielectric substrate is FR-4 where the relative permittivity is 4.4, and loss tangent is 0.02. The thickness of the dielectric substrate is 2 mm.

As shown in Fig. 6(b), our proposed FSS structure is located directly above the MIMO antenna. The distance between them is H and the air layer in the middle. S_{11} curves of the proposed FSS antenna with different H are shown in Fig. 7. When H equals 16 mm, a larger bandwidth of the FSS antenna can be formed. The resonant frequencies of the MIMO antenna are 5.8 GHz and 6.4 GHz, and the working bandwidths are 5.71–6.03 GHz and 6.31–6.52 GHz.

The antenna gain can be improved when FSS is loaded on the antenna. The schematic diagram of FSS enhance antenna gain is shown in Fig. 8. Using partial reflection characteristics of FSS, the electromagnetic waves radiated by the microstrip antenna are reflected many times between the FSS

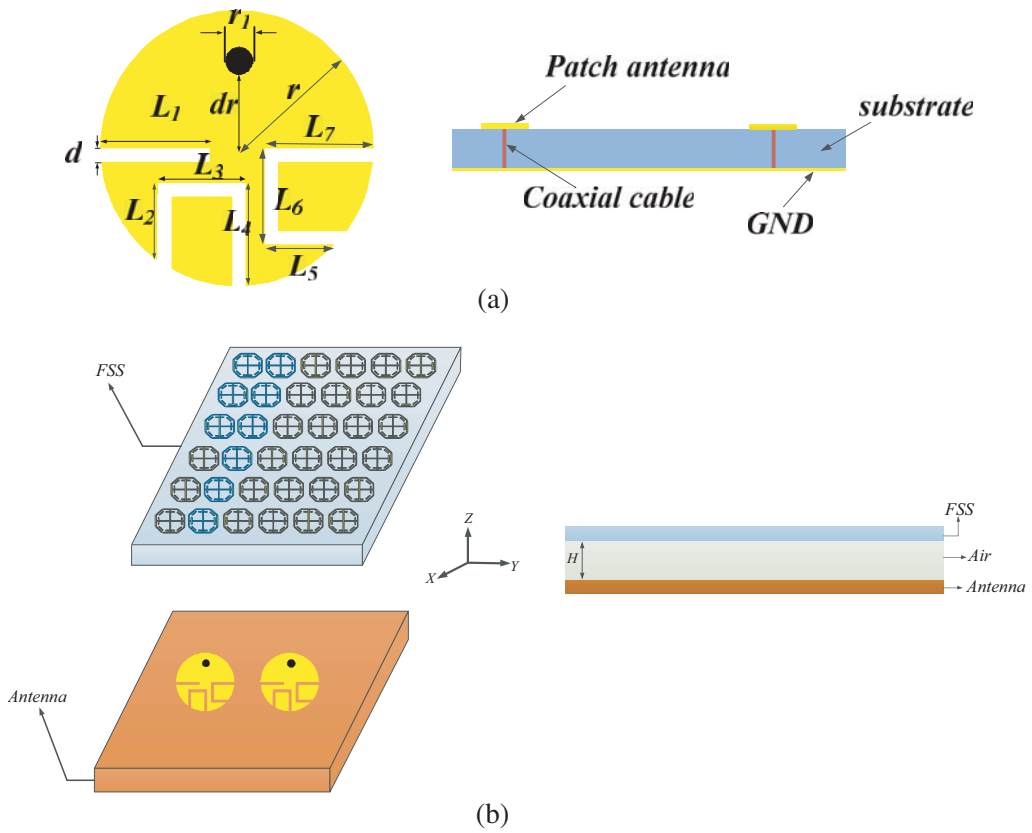

Figure 6. Configuration and parameters of the antenna: $L_1 = 10.5\,\text{mm}$, $L_2 = 7\,\text{mm}$, $L_3 = 8\,\text{mm}$, $L_4 = 10\,\text{mm}$, $L_5 = 7\,\text{mm}$, $L_6 = 8\,\text{mm}$, $L_7 = 10\,\text{mm}$, $d = 0.5\,\text{mm}$, $r = 11.5\,\text{mm}$, $r_1 = 1\,\text{mm}$, $dr = 7.5\,\text{mm}$. (a) Single microstrip patch and (b) configuration of the proposed FSS antenna.

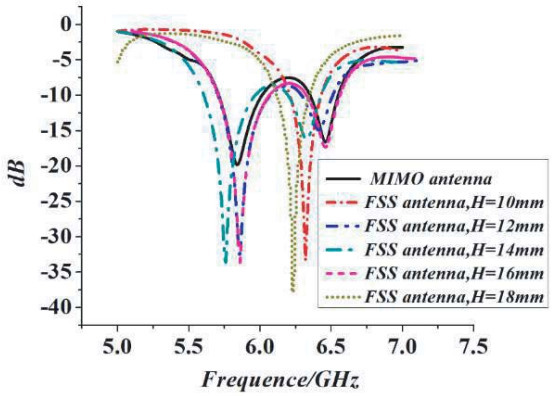

Figure 7. S_{11} curve of FSS structure with MIMO antenna at different distances.

and the ground. Supposing that other losses are not taken into account, the EM wave radiated by the microstrip antenna is

$$P_1(\theta) = \left[1 - \Gamma^2(\theta)\right] F^2(\theta) \tag{6}$$

The phase will be delayed, and the wave loss comes from the ground reflection. The phase of each FSS unit transmitting electromagnetic waves is shown in Eq. (7).

$$P_D = \varphi(\theta) - \pi - \frac{4\pi H}{\lambda \cos\theta} \tag{7}$$

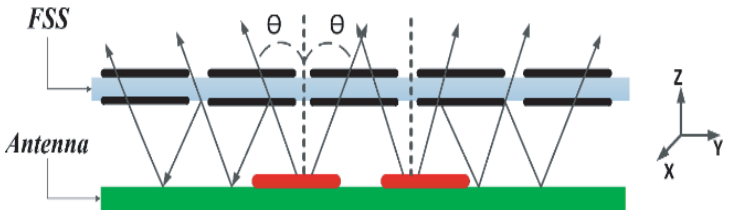

Figure 8. Schematic diagram of FSS enhance antenna gain.

According to the theory of reflection, the radiation power pattern is shown in Eq. (8).

$$P(\theta) = \left[1 - \Gamma^2(\theta)\right] F^2(\theta) \left\{1 + \Gamma^2(\theta) - 2\Gamma(\theta) \cos\left[\varphi(\theta) - \pi - \frac{4\pi H}{\lambda \cos\theta}\right]\right\}^{-1} \tag{8}$$

where λ is the free space wavelength, $\Gamma(\theta)$ the complex representation of the FSS reflection coefficient, and $F(\theta)$ the pattern function of the original antenna.

Since the change of height H and reflection coefficient Γ will lead to the change of the gain, the gain of antenna can be optimized, where Γ is related to the permeability of FSS. Fig. 9 shows the comparisons of radiation patterns of the FSS antenna at different resonant frequencies. It can be seen that the gain of the FSS antenna has been improved, and the maximum 3 dB has been increased for both E and H planes.

Figure 10(a) shows the variation of RCS with incident angle at 5.8 GHz. It can be seen that the RCS in the normal direction of the antenna is well suppressed after loading the FSS. For TM polarization, although the RCS increases by more than 3 dB in the side lobe range of $-140°$ to $-40°$, RCS has a reduction of more than 3 dB in the range of main lobe. It is shown that loading FSS can change the spatial scattering field distribution of the antenna. Accordingly, the RCS value in the main radiation direction of the antenna can be well suppressed.

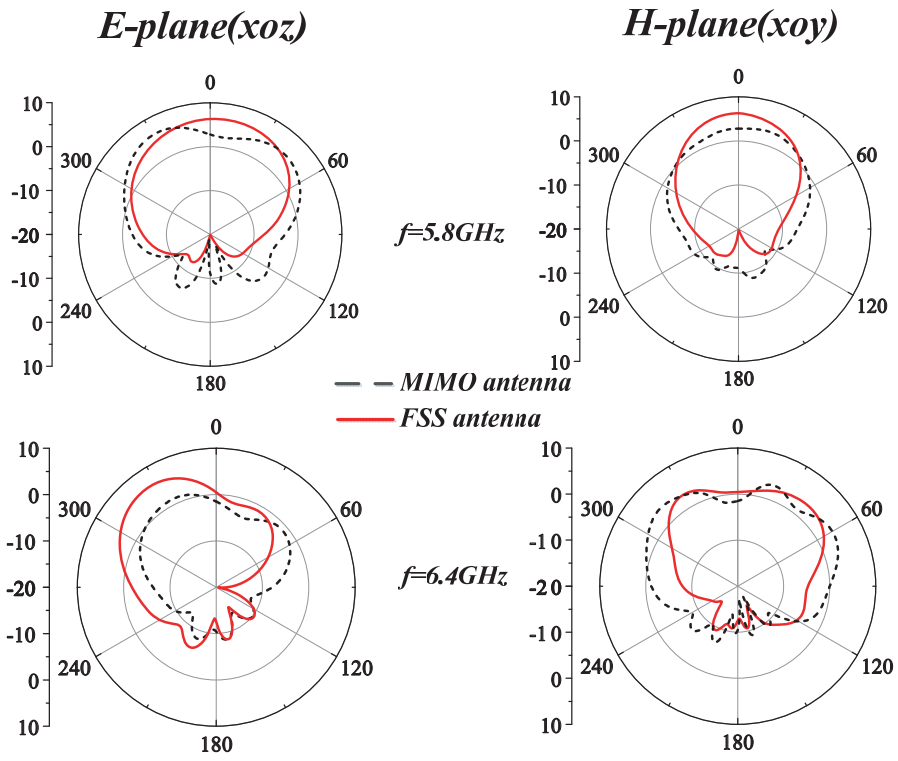

Figure 9. Comparisons of radiation pattern of the MIMO antenna and FSS antenna.

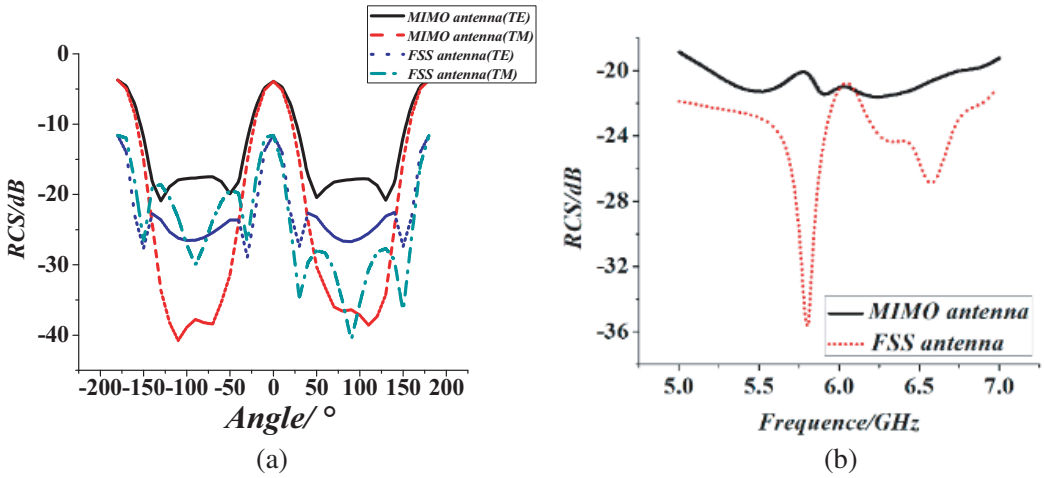

Figure 10. RCS curves of FSS antenna. (a) Comparison of FSS antenna RCS sweep angle and (b) comparison of FSS antenna RCS sweep frequency.

Figure 10(b) shows that RCS of FSS antenna varies with frequency. It can be seen that the RCS of FSS antenna is significantly reduced compared with MIMO antenna in the whole working frequency band, at the maximum reduced 16 dB.

3. MEASURED RESULTS

An image of the fabricated FSS antenna is shown in Fig. 11. The S_{11} curve, E plane and H plane of the antenna are measured by using the Aligent 5071C network analyzer and far-field test method. The simulated and measured S_{11} results of the MIMO antenna and proposed FSS antenna are shown in Fig. 12(a). These results indicate that the -10 dB impedance bandwidth of the MIMO antenna is 5.4% (5.71–6.03 GHz) at the lower frequency and 3.4% (6.31–6.52 GHz) at the higher frequency. The FSS antenna frequency bands reach 7.1% (5.69–6.11 GHz) and 5.1% (6.30–6.63 GHz). Compared to the MIMO antenna, the bandwidth of the proposed FSS antenna is extended by 31.4% at low frequency and 50% at high frequency, respectively. The increase in bandwidth of FSS antenna is mainly due to the new resonance generated by a coupling between FSS structure and MIMO antenna.

The isolation of FSS antenna is shown in Fig. 12(b). It can be seen that the isolation of FSS antenna in the whole working frequency band has been improved compared with MIMO antenna, with a maximum increase of 16 dB. The measured two-dimensional radiation patterns of the proposed FSS antenna at frequencies of 5.8 and 6.4 GHz are shown in Fig. 12(c). The E and H planes are observed,

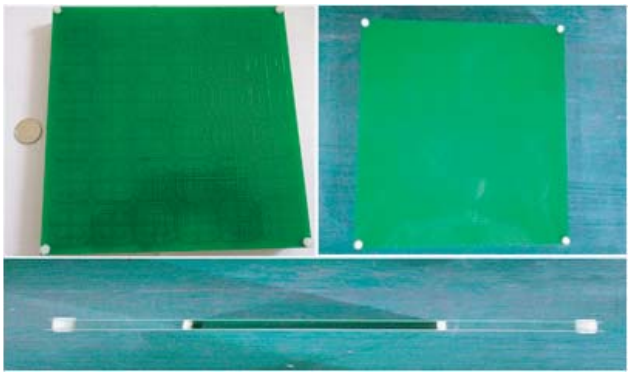

Figure 11. Image of the fabricated MIMO antenna with FSS.

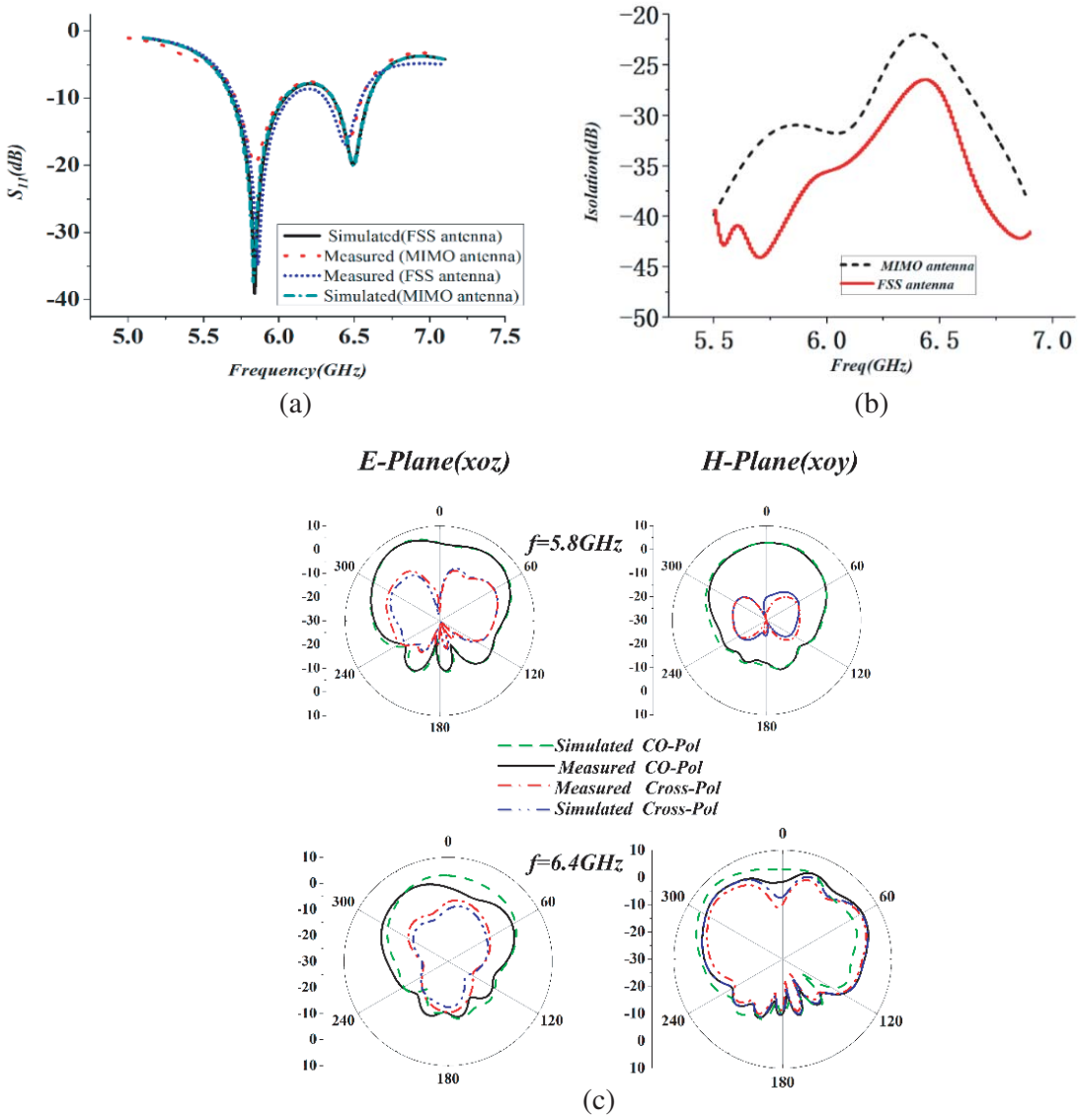

Figure 12. Measured S_{11} and radiation patterns of the FSS antenna. (a) The curve of S_{11}. (b) The curve of S_{21}. (c) radiation pattern.

and the simulation data and test data are basically consistent. The cross-polarization performance of FSS antenna is excellent at 5.8 GHz, and the cross-polarization ratio is greater than −15 dB. Fig. 13 shows the measured peak gains of FSS antenna and MIMO antenna. The data reveal that peak gain enhancements of 2.53 dB at 5.8 GHz and 1.86 dB at 6.4 GHz are achieved by the proposed FSS antenna.

Figure 14 shows that FSS applied in transmission coefficient. The FSS structure has dual-passband, and the transmission of electromagnetic waves will not change in the passband. Fig. 15(a) shows the transmission coefficient for antenna with FSS or without FSS. The amplitude and phase of S_{21} are measured by vector network analyzer.

The antenna working frequency is 2.0–2.69 GHz, and the FSS structure passband is 2.0–3.4 GHz. Thus, FSS will be applied in antenna. The data reveal that FSS transmission passband characteristic is better, and the transmission coefficient of the antenna changes within acceptable limits.

Figure 15(b) shows phase of the antenna with FSS or without FSS. It can be seen that the phase of antenna has no change basically. It is shown that the designed FSS structure has better transmission characteristics.

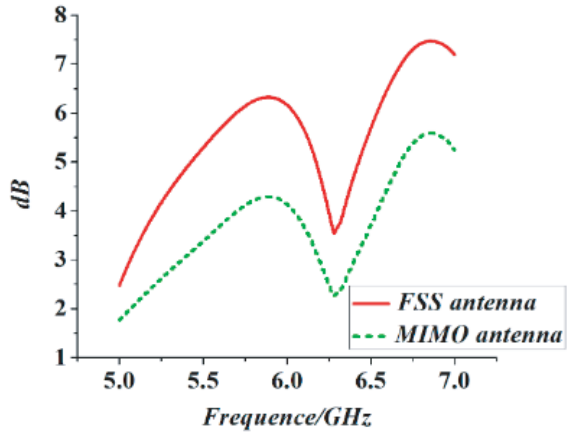

Figure 13. Experimentally measured peak gain of the MIMO antenna and the proposed FSS antenna.

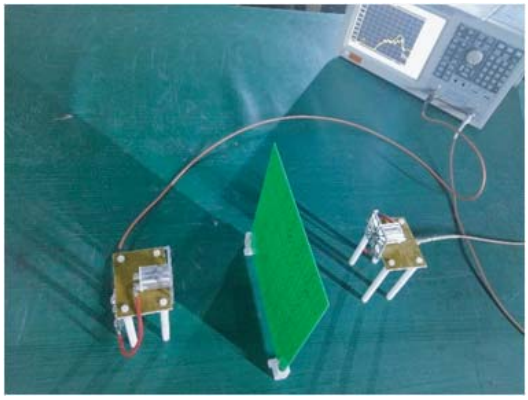

Figure 14. FSS structure application in transmission coefficient.

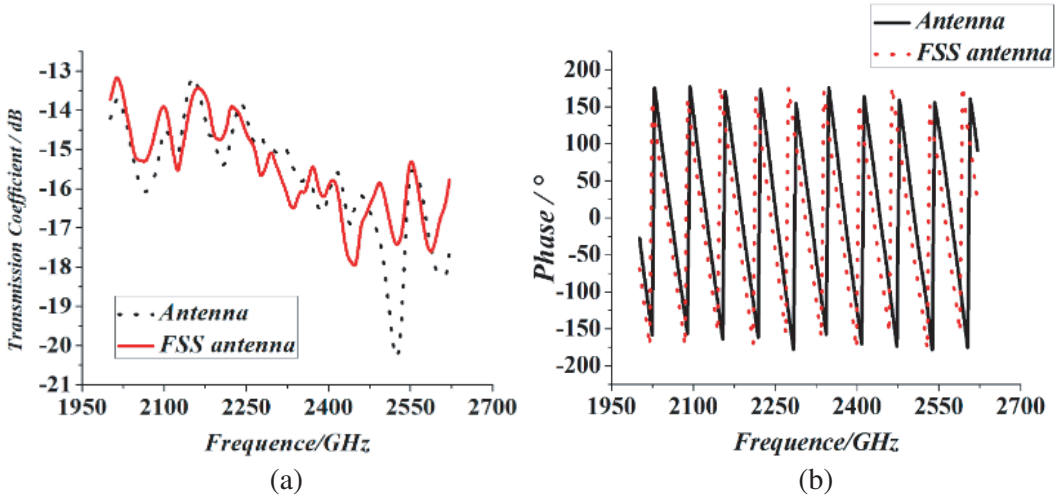

Figure 15. Transmission coefficient and phase of FSS antenna. (a) Transmission coefficient and (b) transmission phase.

4. CONCLUSION

A novel FSS is proposed and fabricated in this manuscript. By adding this proposed FSS structure into MIMO antenna, the performance parameters of the MIMO antenna can be easily enhanced. The measured results show that this fabricated proposed FSS antenna has a wider bandwidth, higher gain and lower RCS than a MIMO antenna. The bandwidth of FSS antenna is extended 31.4% and 50% in low frequency and high frequency, respectively. The peak gain enhancements of 2.53 dB at 5.8 GHz and 1.86 dB at 6.4 GHz are achieved by the proposed FSS antenna. The maximum RCS reduction of proposed FSS antenna is 16 dB. When analyzing the transmission coefficient of our proposed FSS, it can be seen that FSS has better transmission characteristics.

ACKNOWLEDGMENT

This work was supported by the National Natural Science Foundation of China (61601185, 81460275) and Natural Science Foundation of Jiangxi Province (20171ACB21040).

REFERENCES

1. Wu, T. K., *Frequency Selective Surface and Grid Array*, Wiley, 1995.
2. Raspopoulos, M. and S. Stavrou, "Frequency selective buildings through frequency selective surfaces," *IEEE Trans. Antennas Propag.*, Vol. 59, No. 8, 2998–3005, 2011.
3. Kiani, G. I., L. G. Olsson, A. Karlsson, K. P. Esselle, and M. Nilsson "Cross-dipole bandpass frequency selective surface for energy-saving glass used in buildings," *IEEE Trans. Antennas Propag.*, Vol. 59, No. 2, 520–525, 2011.
4. Ranga, Y., L. Matekovits, S. G. Hay, and T. S. Bird, "An anisotropic impedance surface for dual-band linear-to-circular transmission polarization convertor," *International Workshop on Antenna Technology (iWAT)*, 2013.
5. Yeo, W., N. K. Nahar, and K. Sertel, "FAR-Ir multiband dual polarization perfect absorber for wide incident angles," *Microwave and Optical Technology Letters*, Vol. 55, No. 3, 632–636, 2013.
6. Goussetis, G. and A. P. Feresidis, "Perturbed frequency selective surfaces for multiband high impedance surfaces," *IET Microwave Antennas Propagation*, Vol. 4, No. 8, 1105–1110, 2010.
7. Campos, A. L. P. S, S. F. C. G. Segundo, R. H. C. Manic, G. A. Neto, A. G. D. Assunc, "A simple fractal geometry to design multiband frequency selective surfaces," *Microwave and Optical Technology Letters*, Vol. 54, No. 10, 2321–2325, 2012.
8. Jamil, A., M. Z. Yusoff, and N. Yahya, "Compact SRR based band stop filter for isolation in WLAN band in MIMO," *IEEE Student Conference on Research and Development*, 370–373, 2013.
9. Zhong, J., Y. Huang, G. Wen, H. Sun, O. Gordon, and W. Zhu, "Dual-band negative permittivity metamaterial based on cross circular loop resonator with shorting stubs," *IEEE Antennas and Wireless Propagation Letters*, Vol. 11, 803–806, 2012.
10. Miyamaru, F., S. Kubota, and T. Nakanishi, "Transmission properties of double-gap asymmetric split ring resonators in terahertz region," *Applied Physics Letters*, Vol. 101, No. 5, 051112-1–051112-5, 2011.
11. Lahiri, B., S. G. McMeekin, and R. M. De La Rue, "Resonance hybridization in nano antenna arrays based on asymmetric split-ring resonators," *Applied Physics Letters*, Vol. 98, No. 15, 153116-1–153116-3, 2011.
12. Costa, F., A. Monorchio, and G. Manara, "Efficient analysis of frequency-selective surfaces by a simple equivalent-circuit model," *IEEE Antennas Propagation Magazine*, Vol. 54, No. 4, 35–48, 2012.
13. Kim, G. and B. Hong, "An object transition flow model of test data set for simulation of RFID applications," *IEEE International Conference on e-Business Engineering (ICEBE)*, 2014.

14. Huang, H., P. Zhao, P.-Y. Chen, Y. Ren, X. Liu, M. Ferrari, H. Ye, and D. Akinwande, "RFID tag helix antenna sensors for wireless drug dosage monitoring," *IEEE Translational Engineering in Health and Medicine*, Vol. 2, No. 2, 1700108-1–1700108-8, 2014.
15. Lazaro, A., A. Ramos, D. Girbau, and R. Villarino, "A novel UWB RFID tag using active frequency selective surface," *IEEE Transactions on Antennas and Propagation*, Vol. 61, No. 3, 1155–1164, 2013.
16. Carelli, P., F. Chiarello, S. Cibella, G. A. Di, R. Leoni, M. Ortolani, and G. Torrioli, "A fast terahertz spectrometer based on frequency selective surface filters," *Infrared Milli. Terahz. Waves*, Vol. 33, No. 3, 505–512, 2012.
17. De Lima E Silva, T. and A. L. P. S. Campos, "Formulation of double screen FSS analysis using Fullwave method," *IEEE Microwave Optoelectronics Conference*, 512–516, 2012.
18. Silva, T. D. L. E. and A. L. P. S. Campos, "Formulation of double screen FSS analysis using Fullwave method," *IEEE Microwave Optoelectronics Conference*, 512–516, 2012.
19. Majumdar, P., Z. Zhao, and C. Ji, "Equivalent circuit model of multilayer double square loop FSS using vector-fitting," *IEEE International Symposium on Antennas and Propagation*, 1276–1277, 2015.